





# Super-Resolution Imaging with Patchy Microspheres

Qingqing Shang <sup>1,†</sup>, Fen Tang <sup>2,3,†</sup>, Lingya Yu <sup>4</sup>, Hamid Oubaha <sup>5</sup>, Darwin Caina <sup>5,6</sup>, Songlin Yang <sup>7</sup>, Sorin Melinte <sup>5</sup> , Chao Zuo <sup>8</sup> , Zengbo Wang <sup>4</sup>  and Ran Ye <sup>2,3,8,\*</sup> 

- <sup>1</sup> Key Laboratory for Opto-Electronic Technology of Jiangsu Province, Nanjing Normal University, Nanjing 210023, China; 201043036@njnu.edu.cn  
<sup>2</sup> School of Computer and Electronic Information, Nanjing Normal University, Nanjing 210023, China; 201043034@njnu.edu.cn  
<sup>3</sup> School of Artificial Intelligence, Nanjing Normal University, Nanjing 210023, China  
<sup>4</sup> School of Computer Science and Electronic Engineering, Bangor University, Bangor LL57 1UT, UK; yulingya0408@gmail.com (L.Y.); z.wang@bangor.ac.uk (Z.W.)  
<sup>5</sup> Institute of Information and Communication Technologies, Electronics and Applied Mathematics, Université Catholique de Louvain, 1348 Louvain-la-Neuve, Belgium; hamid.oubaha@uclouvain.be (H.O.); darwin.caina@uclouvain.be (D.C.); sorin.melinte@uclouvain.be (S.M.)  
<sup>6</sup> Faculty of Science, Universidad Central del Ecuador, Quito 170521, Ecuador  
<sup>7</sup> Advanced Photonics Center, Southeast University, Nanjing 210096, China; yangsonglin@seu.edu.cn  
<sup>8</sup> Smart Computational Imaging Laboratory (SCILab), School of Electronic and Optical Engineering, Nanjing University of Science and Technology, Nanjing 210094, China; zuochao@njnu.edu.cn  
\* Correspondence: ran.ye@njnu.edu.cn  
† These authors contributed equally to this work.

**Abstract:** The diffraction limit is a fundamental barrier in optical microscopy, which restricts the smallest resolvable feature size of a microscopic system. Microsphere-based microscopy has proven to be a promising tool for challenging the diffraction limit. Nevertheless, the microspheres have a low imaging contrast in air, which hinders the application of this technique. In this work, we demonstrate that this challenge can be effectively overcome by using partially Ag-plated microspheres. The deposited Ag film acts as an aperture stop that blocks a portion of the incident beam, forming a photonic hook and an oblique near-field illumination. Such a photonic hook significantly enhanced the imaging contrast of the system, as experimentally verified by imaging the Blu-ray disc surface and colloidal particle arrays.

**Keywords:** photonic jet; photonic hook; patchy particle; microspheres; super-resolution imaging



**Citation:** Shang, Q.; Tang, F.; Yu, L.; Oubaha, H.; Caina, D.; Yang, S.; Melinte, S.; Zuo, C.; Wang, Z.; Ye, R. Super-Resolution Imaging with Patchy Microspheres. *Photonics* **2021**, *8*, 513. <https://doi.org/10.3390/photonics8110513>

Received: 10 October 2021  
Accepted: 8 November 2021  
Published: 15 November 2021

**Publisher's Note:** MDPI stays neutral with regard to jurisdictional claims in published maps and institutional affiliations.



**Copyright:** © 2021 by the authors. Licensee MDPI, Basel, Switzerland. This article is an open access article distributed under the terms and conditions of the Creative Commons Attribution (CC BY) license (<https://creativecommons.org/licenses/by/4.0/>).

## 1. Introduction

Optical microscopes (OMs) are one of the most important tools for scientific research. Due to the Abbe diffraction limit, conventional OMs cannot resolve two objects closer than  $0.5\lambda/NA$ , where  $\lambda$  is the incident wavelength and NA is the numerical aperture of the microscope. Therefore, an OM equipped with a near-unity NA objective and a white light source ( $\lambda \sim 550\text{--}600$  nm) has a resolution limit of 300 nm. Within this context, many different methods have been proposed to overcome this limitation. In 2009, Lee et al. successfully used nanoscale spherical lenses to resolve features beyond the diffraction limit [1]. Later, Wang et al. demonstrated the super-resolution imaging of 50 nm features using dielectric microspheres under white light illumination [2]. Smaller features, i.e., 15–25 nm nanogaps, can be resolved with microspheres under a confocal microscope [3,4]. Since the resolution of an imaging system is often measured by the point spread function (PSF) instead of by the resolved feature size, Allen et al. developed a convolution-based resolution analysis method and derived the best resolution for microsphere nanoscopy is  $\sim\lambda/6-\lambda/7$  [4]. Microsphere-assisted imaging has the advantages of simple operation, no fluorescent labeling, and good compatibility with commercial OMs. To obtain high-quality images, various parameters affecting the imaging performance of microspheres have

been studied, such as illumination conditions [5], microsphere diameters [6], immersion mode [7–9], and immersion materials [10–12].

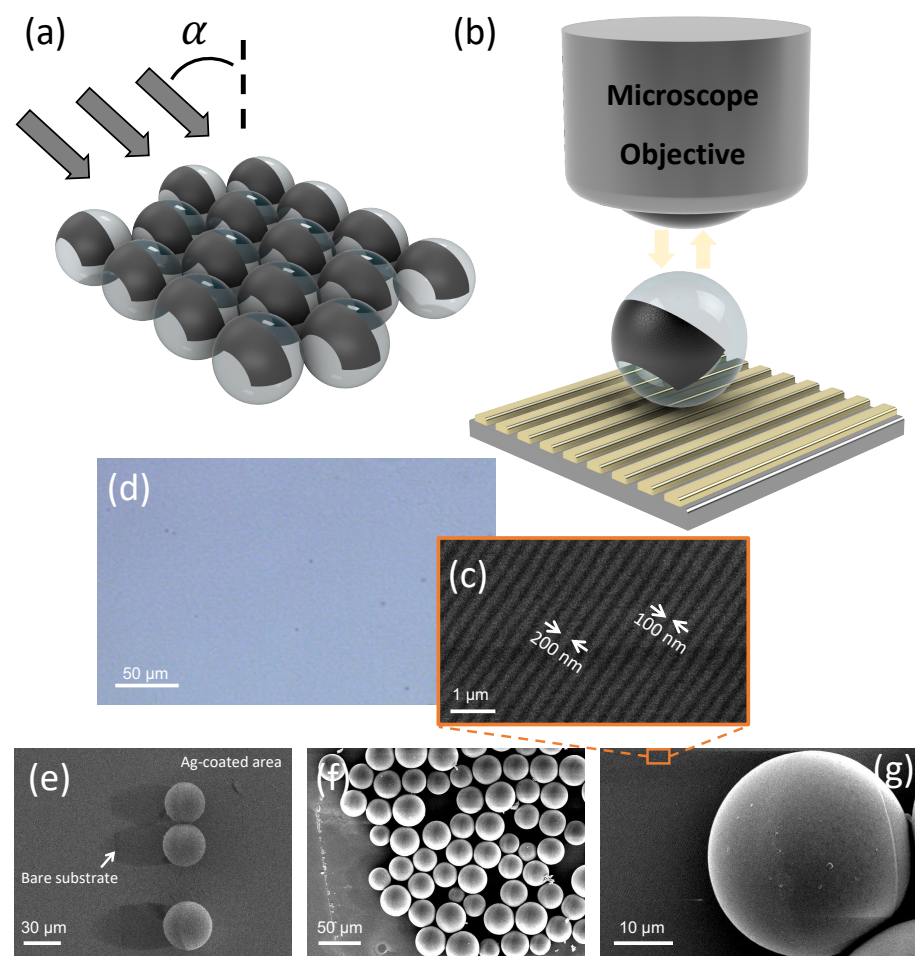
Currently, most microsphere-assisted imaging methods use high-refractive-index microspheres in a liquid environment [13–17]. Nevertheless, the imaging performance of the microspheres can be affected by the shape of air–liquid interfaces as well as the refractive index distribution of liquid films. Moreover, samples may be contaminated or even damaged in liquid. Only a small amount of research has been done to improve the imaging performance of microspheres in air, such as improving illumination conditions [5], optimizing the diameter and the refractive index of microspheres [18], using plano-convex-microsphere (PCM) lens design [19,20], and using a microsphere lens group [21].

Patchy particles are anisotropic particles having two or more different physical or chemical properties on their surfaces. They are considered as promising materials for biomedical, environmentally friendly, and sustainable applications, such as biosensing, drug delivery, water decontamination, hydrogen production, etc. [22,23]. Patchy particles are also a type of optical functional materials. For example, the mirror made of Ag-coated patchy particles can have optical responses to external electric and magnetic fields, and its optical reflectivity can be adjusted in real-time by changing the external fields [24]. Here we present the performance of super-resolution imaging in air using patchy microspheres. To the best of our knowledge, this is the first study showing that patchy microspheres are suitable for super-resolution imaging. The patchy particles can generate a curved photonic jet, i.e., photonic hook, due to their structural asymmetry [25–27], which is shown to be useful in boosting the imaging contrast and quality in this work. The results will contribute to the further advancement of the microsphere-based optical nanoscopy/microscopy techniques and facilitate their applications in nanotechnology, life sciences, etc.

## 2. Materials and Methods

Figure 1a illustrates the schematic drawing of the patchy microsphere fabrication by glancing angle deposition (GLAD) method [28]. BaTiO<sub>3</sub> glass (BTG, 27–35 μm diameter,  $n = 1.9$ , Microspheres-Nanospheres, USA) were self-assembled into monolayers by drop-casting a small amount of BTG powders on a glass slide followed by using water to compact them together. The microsphere arrays were then coated with 100 nm thick Ag films by physical vapor deposition (PVD) (1 Å/s) at a constant angle ( $\alpha = 60^\circ$ ). We chose Ag because it has been used in microsphere-assisted microscopy to modify the optical properties of the substrate on which the sample is fixed [29] or the sample itself [30], in order to achieve the desired imaging quality. After deposition, a stream of deionized water was used to transfer the microspheres from the glass slide to the observation sample. We call the fabricated patchy BTG microspheres p-BTG particles.

The p-BTG particles were observed with a commercial reflected light microscope (Axio AX10, Carl Zeiss) for super-resolution imaging (Figure 1b). The microspheres collected near-field nanoscale information from a Blu-ray disk (BD) surface and generated a magnified real image above the sample, which was then captured by the objective lens. This is confirmed by the imaging plane that is above the substrate, in contrast to virtual imaging whose image plane is down into the substrate. The entire imaging process was performed in air. A 20 × objective (NA = 0.4, EC EPIPLAN, Carl Zeiss) was used for imaging with the p-BTG particles. The system was illuminated by a white light source (HAL 100, Carl Zeiss). All the experimental results were recorded using a high-speed scientific complementary metal-oxide-semiconductor (CMOS) camera (DFC295, Leica). The Leica Application Suite X (LAS X) software was used to take optical microscopic images with the camera and to measure the intensity profiles from the recorded images. The magnification factor (M) was obtained by dividing the period of the intensity profiles by the period of the BD pattern.



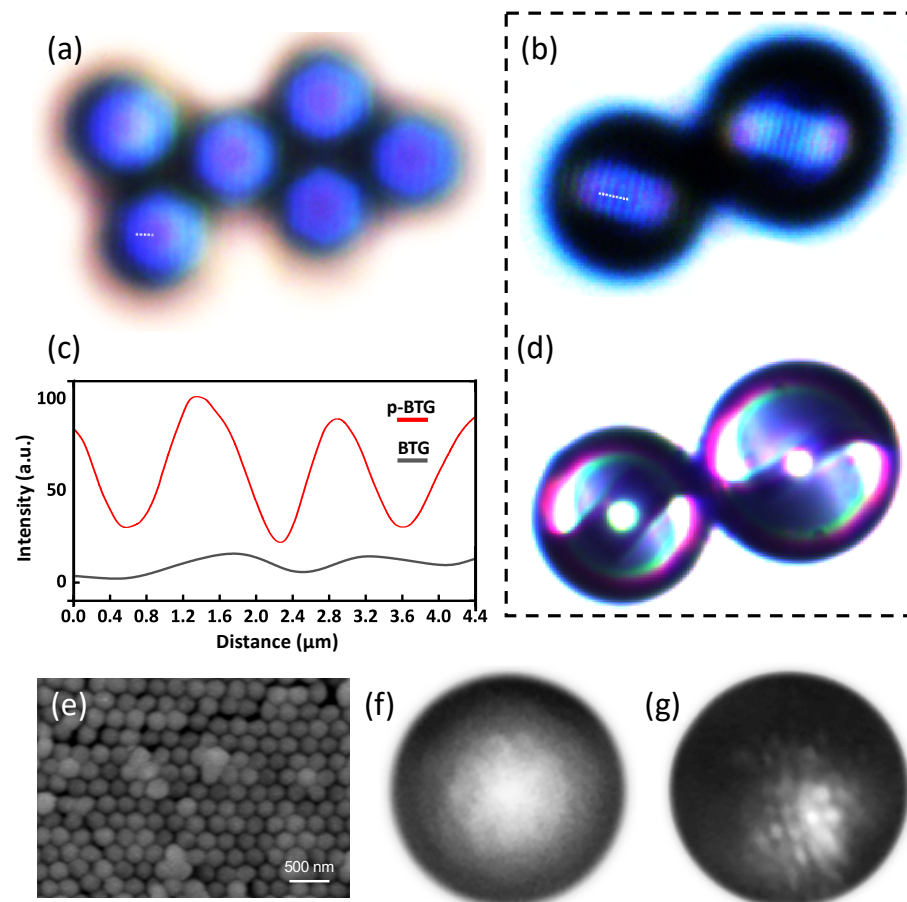
**Figure 1.** (a) Fabrication of patchy BTG (p-BTG) particle by glancing angle deposition method; (b) experimental setup of super-resolution imaging with p-BTG lens; (c) SEM image and (d) OM image of BD substrate (lines not resolved); (e,f) SEM images of p-BTG particle after Ag deposition; (g) SEM image of p-BTG particle transferred on BD substrate.

Figure 1c shows the scanning electron microscopic (SEM) image of the top surface of the BD sample in this study. It has a strip pattern with 300 nm periodicity, including 200 nm track width and 100 nm gap between two adjacent tracks. The pattern of the BD cannot be resolved by conventional OM method with diffraction-limited resolution of  $\lambda/2NA = 550/0.8 = 687.5$  nm (Figure 1d). The p-BTG microspheres after depositing 100 nm Ag by the GLAD method ( $\alpha = 60^\circ$ ) are shown in Figure 1e. There are some elliptical shadows on the left side of the microspheres (white arrow, Figure 1e), because the microspheres blocked the transportation of Ag vapor from the source to the substrate during deposition. The corresponding SEM image of the p-BTG particle arrays also confirms the presence of Ag patches on the microspheres (Figure 1f). Figure 1g shows a p-BTG on a BD sample, in which both the Ag patch and the strip pattern can be observed.

### 3. Results and Discussion

In this study, the imaging performance of BTG and p-BTG microlenses in air were compared with each other. As shown in Figure 2a, the BTG particle in air formed a magnified, low-contrast, real image of the strip pattern above the BD. The gap between the two neighboring tracks was  $2.5 \mu\text{m}$  at the clearest image position, corresponding to a M of  $\sim 8.3\times$ . Here, the super-resolution image formed by the BTG microsphere has a poor quality, with very low imaging contrast, which is not sufficient for most of the practical applications. On the contrary, as shown in Figure 2b, the new p-BTG microspheres generate significantly improved super-resolution images, both in quality and contrast. The imaging

contrast has been boosted by a factor of  $\sim 6.5$ , as shown in Figure 2c by retrieved intensity profiles along the white dash lines in Figure 2a,b. The measured magnification factor for the p-BTG lens is about  $3.9\times$ , which is smaller than that of unpatched particles ( $M = 8.3\times$ ). This is caused by different focusing characteristics of BTG and p-BTG particles which will be discussed below.



**Figure 2.** (a,b) OM images of the pattern on BD surface observed through (a) pristine BTG and (b) p-BTG with the  $20\times$  objective; (c) optical intensity profiles across the white dash lines; (d) OM image of the corresponding p-BTG; (e) SEM image of the 230 nm-diameter SiO<sub>2</sub> particle arrays; (f,g) the SiO<sub>2</sub> particle arrays observed through (f) pristine BTG and (g) p-BTG microspheres.

Interestingly, as shown in Figure 2d, we observed two patchy textured patterns in each p-BTG particle, but only one side of the microspheres was coated with Ag films. The two paired patterns have a rotation angle of  $180^\circ$  between them around the center of the microsphere. This phenomenon could be attributed to the internal reflection occurring inside the high-index microspheres, in which case the Ag film prevents part of the incident light from entering the microsphere and causes a shadow with the same shape on the other side of the microsphere after multiple internal reflections.

In another imaging test, silica particles with 230 nm mean diameter (Nanorainbow Biotechnology, Nanjing, China) were self-assembled into arrays (Figure 2e) [31,32] and observed through BTG and p-BTG particles in air. The silica particle arrays were coated with 20 nm Ag before observation to enhance their reflectivity. As shown in Figure 2f,g, the p-BTG particle again demonstrates a better imaging performance over the BTG particle when imaging a sub-diffraction-limited nanoparticle array.

In our experiments, we found that the p-BTG particles deposited on the sample surface may have different appearances: bright, dark, or textured, and different imaging performance, depending on the positions of Ag coatings. As shown in Figure 3a, when

the Ag film is at the bottom of the microsphere, it is like a concave mirror that reflects the incident light backward in a convergent way, so that more light can be collected by the objective, leading to a bright appearance. On the contrary, the p-BTG looks dark when the Ag film is on top of the microsphere. As shown in Figure 3b, the Ag film acts like a convex mirror that reflects the incident beam divergently at a large angle, so that most of the reflected light cannot be captured by the objective. The p-BTG lens shows a textured appearance and forms a magnified real image when the Ag film is on the side of the microsphere (Figure 3c), in which case the Ag film acts as an aperture stop, enhancing the contrast of the image and forming a photonic hook inside the microsphere. However, in this work the patchy particles have an uncontrolled movement during the water-flow-assisted transfer process, the position of the Ag coatings is random after the transfer step, so we took pictures of patchy particles with various appearances, and selected the most representative ones to be shown in Figure 3, in order to explain the observed optical phenomenon. Techniques such as probe-based microscale manipulation can be used to precisely control the positions of the Ag films in the future. In addition, we found that coating BTG particles with aluminum patches also can improve the microsphere's imaging contrast (Supplementary Materials Figure S1).

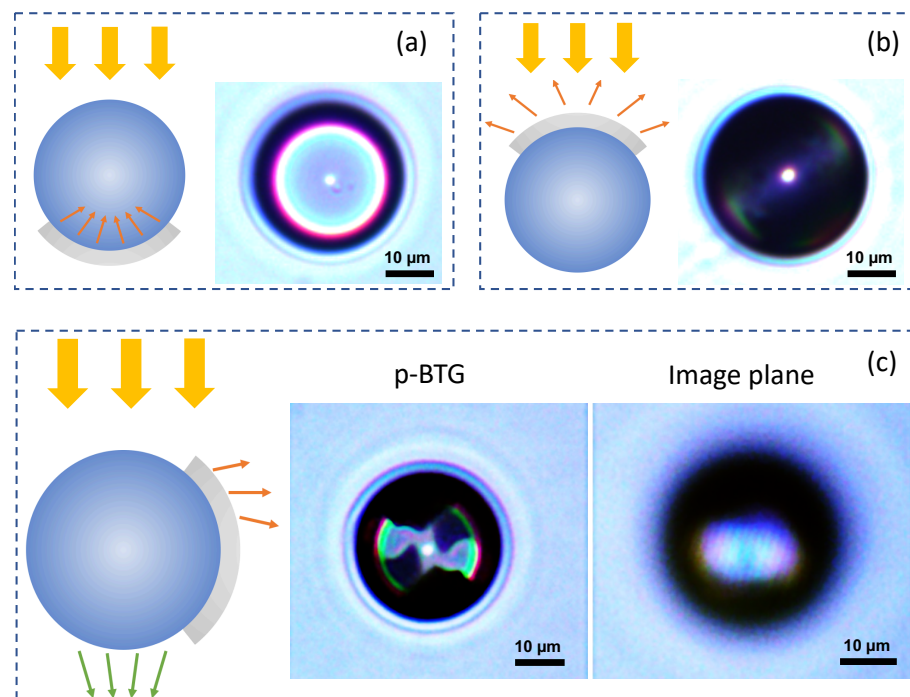


**Figure 3.** OM images of p-BTG particles when the Ag film is (a) at bottom of the microsphere, (b) on top of the microsphere, and (c) on the side of the microsphere.

To understand the main focusing properties of the p-BTG microsphere lens, computational modeling was performed on a workstation (HP Z8, 125 GB random access memory) using the two-dimensional (2D) finite-difference-time-domain (FDTD) method with Lumerical FDTD Solutions. 2D modeling is a commonly used method to investigate the light field around dielectric particles [25,27], because 3D sphere modeling is usually not possible due to the limited computing resource. As shown in Figure 4a,b, cylinders ( $D = 35 \mu\text{m}$ ,  $n_1 = 1.9$ ) were created for the FDTD simulation. The background medium was set to air ( $n_2 = 1$ ). The area with the largest field intensity is considered as the focal point. The distance between the focal point and the bottom edge of the particle is defined as FP, which is positive when the focus is outside of the cylinder, and negative otherwise. As shown in Figure 4a, a plane light ( $\lambda = 550 \text{ nm}$ ) propagating in the Y direction forms a photonic jet inside the cylinder. Figure 4b is the FDTD simulation result of the intensity field distribution in the vicinity of a cylinder partially covered with a 100 nm thick Ag film ( $\beta = 90^\circ$ ,  $\theta = 10^\circ$ ). We can see

the formation of a “photonic hook”, with the light path off-centered and curved due to the asymmetry property of the incident beam caused by the Ag coating. In terms of imaging, the oblique illumination can help the lens to capture higher orders of diffraction from the sample [33] and enhance the phase contrast [34], which turned out to be very beneficial in boosting the quality and the contrast in microsphere-based super-resolution imaging. This enhancement mechanism can play an important role in developing more advanced and reliable microsphere super-resolution imaging systems.

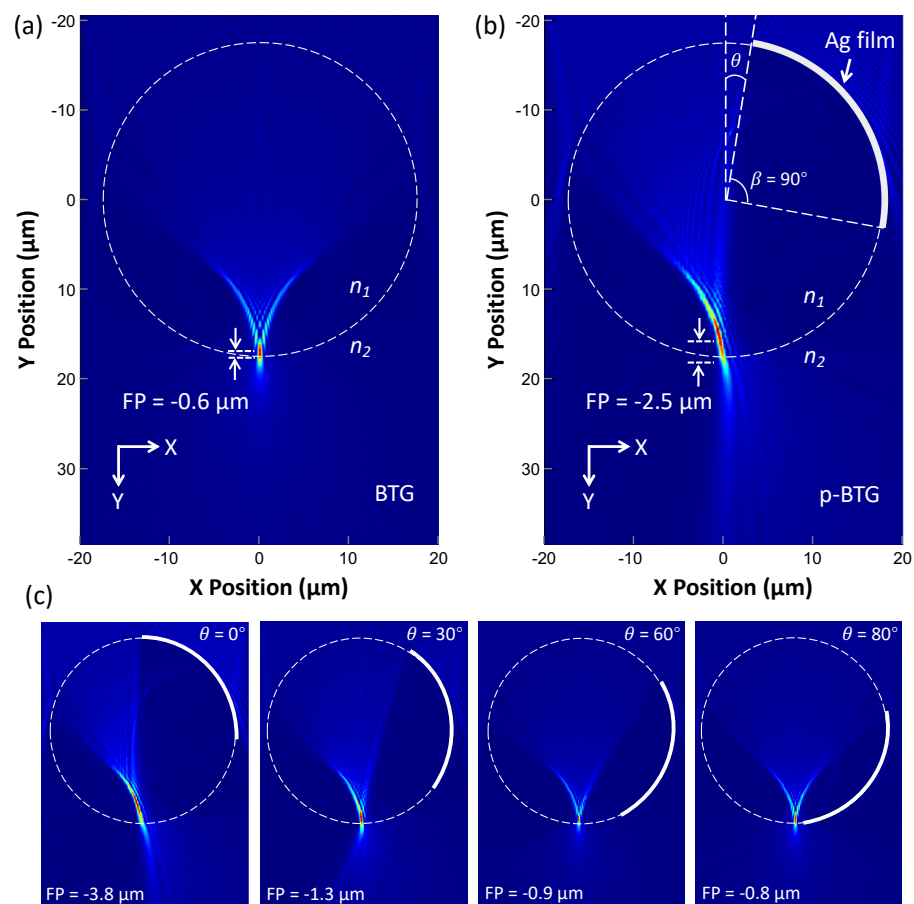


**Figure 4.** (a,b) FDTD-simulated light field of (a) the pristine BTG and (b) the p-BTG; (c) the influence of the position of Ag films on the focusing of the p-BTG.

From Figure 4b we can also see the angled “photonic hook” beam leads to a larger object-to-focus distance (O). Since magnification  $M = I/O$ , where I is the image plane position and O is the object plane position, increasing O will lead to decreased M which can explain why the p-BTG lens produces a smaller magnification factor as in experiments.

To illustrate the position effect of Ag films on BTG particle focusing, we varied the  $\theta$  angle in Figure 4b from  $0^\circ$  to  $80^\circ$ , while keeping the opening angle  $\beta$  of the film coating as  $90^\circ$ . As shown in Figure 4c, the photonic hook phenomenon is maximized at  $\theta = 0$ , which gradually decreases as  $\theta$  increases up to  $60^\circ$ . After this angle, the focusing does not show a curved hook focusing effect. Increasing  $\theta$  from  $0^\circ$  to  $80^\circ$  makes the focus move toward the bottom edge of the cylinder. When  $\theta$  is over  $90^\circ$ , the incident light is reflected back by the silver film and cannot reach the shadow side of the microsphere to illuminate the object (Figure S2). In our experiments, the p-BTG particle with  $\theta$  between  $10^\circ$  and  $45^\circ$  degrees is recommended for overall best performance which is a balanced choice between magnification factor and imaging contrast enhancement.

The focusing of the pristine and patchy particles was also studied with the ray-tracing method using the same model as for the FDTD simulation. A commercial software (TracePro, LAMBDA) was used to perform the simulation. As shown in Figure 5, the FP of the p-BTG has

an approximately constant value of  $\sim 0.95 \mu\text{m}$  as the rotation angle  $\theta$  of the Ag film increases from  $0^\circ$  to  $80^\circ$ . When  $\theta$  is between  $60^\circ$  (Figure 5e) and  $80^\circ$  (Figure 5f), the p-BTG cylinders have a focusing performance similar to that of the pristine BTG (Figure 5a). Compared with the FDTD simulation, the ray tracing shows a longer focal length and the focus is outside of the particles. This difference has been discussed in the published literature [1,2], which reported that when particle size reduces to the super-resolution size window, the particle will have remarkably short near-field focal length [1], and geometrical ray tracing will become invalid and fail to predict the imaging properties for those super-resolution spheres, because light beams propagating through such small spheres could form optical vortices and singularities inside the sphere [2].

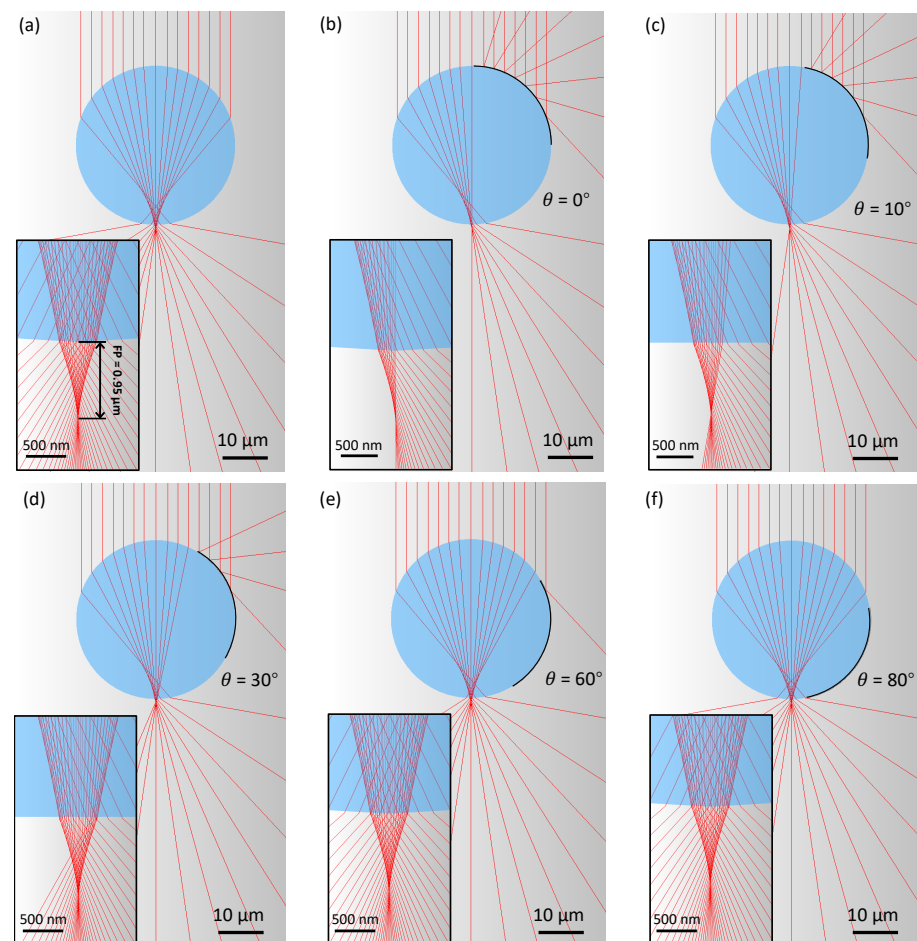


**Figure 5.** The focusing of pristine and patchy BTG particles in air simulated with the ray tracing method: (a) a pristine BTG; (b–f) p-BTG particles with Ag films at a rotation angle of (b)  $\theta = 0^\circ$ , (c)  $\theta = 10^\circ$ , (d)  $\theta = 30^\circ$ , (e)  $\theta = 60^\circ$ , and (f)  $\theta = 80^\circ$ . The inset figures show the corresponding focal points.

In conclusion, BTG microspheres with patchy coating on their surface can provide a new strategy for improving the quality of super-resolution images obtained with high-index microspheres in air. Due to the formation of photonic hook illumination condition, the super-resolution imaging contrast can be improved by a factor of  $\sim 6.5$ , which significantly boosts the overall imaging quality. This method enables achieving high-quality super-resolution imaging without the use of immersion liquid, such as water or oil, opening a new path to developing more advanced and reliable nano-imaging systems based on engineered microsphere lenses. The method proposed in this work is in the early stages. To make a rational design of the decorated microlenses, we still need to understand the effects of the physical parameters (deposition material, film thickness, surface roughness,

etc.) and the geometrical parameters (position, shape, area, etc.) of patches on microspheres' imaging performance. It is also important to develop compatible micromanipulators for the practical applications of the imaging system.

**Supplementary Materials:** The following are available at <https://www.mdpi.com/article/10.3390/photonics8110513/s1>, Figure S1: Optical microscopic image of a Blu-ray disc observed through an aluminum-coated BTG microsphere; Figure S2: The FDTD-simulated light field of a patchy cylinder with an opening angle  $\beta$  of  $90^\circ$  and a rotation angle  $\theta$  of  $120^\circ$ .

**Author Contributions:** Conceptualization, R.Y.; methodology, F.T., Q.S., and R.Y.; software, L.Y. and F.T.; validation, Z.W., C.Z., and R.Y.; formal analysis, F.T., Q.S. and L.Y.; writing—original draft preparation, H.O., D.C., and R.Y.; supervision, C.Z. and R.Y.; funding acquisition, F.T., S.Y., S.M., C.Z., and R.Y. All authors have read and agreed to the published version of the manuscript.

**Funding:** This research was funded by National Natural Science Foundation of China (62105156), Post-graduate Research & Practice Innovation Program of Jiangsu Province (SJCX21\_0580, KYCX21\_0102), European Regional Development Fund (SPARCII-c81133).

**Data Availability Statement:** The data presented in this study are available on request from the corresponding author.

**Acknowledgments:** The support of Fonds Européen de développement régional (FEDER) and the Walloon region under the Operational Program “Wallonia-2020.EU” (project CLEARPOWER) is gratefully acknowledged.

**Conflicts of Interest:** The authors declare no conflict of interest.

## References

1. Lee, J.Y.; Hong, B.H.; Kim, W.Y.; Min, S.K.; Kim, Y.; Jouravlev, M.V.; Bose, R.; Kim, K.S.; Hwang, I.C.; Kaufman, L.J.; et al. Near-field focusing and magnification through self-assembled nanoscale spherical lenses. *Nature* **2009**, *460*, 498–501. [[CrossRef](#)]
2. Wang, Z.; Guo, W.; Li, L.; Luk'Yanchuk, B.; Khan, A.; Liu, Z.; Chen, Z.; Hong, M. Optical virtual imaging at 50 nm lateral resolution with a white-light nanoscope. *Nat. Commun.* **2011**, *2*, 218. [[CrossRef](#)] [[PubMed](#)]
3. Yan, Y.; Li, L.; Feng, C.; Guo, W.; Lee, S.; Hong, M.H. Microsphere-coupled scanning laser confocal nanoscope for sub-diffraction-limited imaging at 25 nm lateral resolution in the visible spectrum. *ACS Nano* **2014**, *8*, 1809–1816. [[CrossRef](#)] [[PubMed](#)]
4. Allen, K.W.; Farahi, N.; Li, Y.; Limberopoulos, N.I.; Walker, D.E.; Urbas, A.M.; Liberman, V.; Astratov, V.N. Super-resolution microscopy by movable thin-films with embedded microspheres: Resolution analysis. *Ann. Phys.* **2015**, *527*, 513–522. [[CrossRef](#)]
5. Perrin, S.; Li, H.; Leong-Hoi, A.; Lecler, S.; Montgomery, P. Illumination conditions in microsphere-assisted microscopy. *J. Microsc.* **2019**, *274*, 69–75. [[CrossRef](#)]
6. Guo, M.; Ye, Y.H.; Hou, J.; Du, B. Size-dependent optical imaging properties of high-index immersed microsphere lens. *Appl. Phys. B-Lasers Opt.* **2016**, *122*, 15. [[CrossRef](#)]
7. Darafsheh, A.; Walsh, G.F.; Negro, L.D.; Astratov, V.N. Optical super-resolution by high-index liquid-immersed microspheres. *Appl. Phys. Lett.* **2012**, *101*, 141128. [[CrossRef](#)]
8. Wang, F.; Yang, S.; Ma, H.; Shen, P.; Wei, N.; Wang, M.; Xia, Y.; Deng, Y.; Ye, Y.H. Microsphere-assisted super-resolution imaging with enlarged numerical aperture by semi-immersion. *Appl. Phys. Lett.* **2018**, *112*, 023101. [[CrossRef](#)]
9. Zhou, Y.; Tang, Y.; He, Y.; Liu, X.; Hu, S. Effects of immersion depth on super-resolution properties of index-different microsphere-assisted nanoimaging. *Appl. Phys. Express* **2018**, *11*, 032501. [[CrossRef](#)]
10. Lee, S.; Li, L.; Wang, Z.; Guo, W.; Yan, Y.; Wang, T. Immersed transparent microsphere magnifying sub-diffraction-limited objects. *Appl. Opt.* **2013**, *52*, 7265–7270. [[CrossRef](#)]
11. Hao, X.; Kuang, C.; Liu, X.; Zhang, H.; Li, Y. Microsphere based microscope with optical super-resolution capability. *Appl. Phys. Lett.* **2011**, *99*, 10–13. [[CrossRef](#)]
12. Ye, R.; Ye, Y.-H.; Ma, H.F.; Cao, L.; Ma, J.; Wyrowski, F.; Shi, R.; Zhang, J.-Y. Experimental imaging properties of immersion microscale spherical lenses. *Sci. Rep.* **2014**, *4*, 3769. [[CrossRef](#)]
13. Ye, R.; Ye, Y.H.; Ma, H.F.; Ma, J.; Wang, B.; Yao, J.; Liu, S.; Cao, L.; Xu, H.; Zhang, J.Y. Experimental far-field imaging properties of a  $\sim 5\text{-}\mu\text{m}$  diameter spherical lens. *Opt. Lett.* **2013**, *38*, 1829–1831. [[CrossRef](#)]
14. Hou, B.; Xie, M.; He, R.; Ji, M.; Trummer, S.; Fink, R.H.; Zhang, L. Microsphere assisted super-resolution optical imaging of plasmonic interaction between gold nanoparticles. *Sci. Rep.* **2017**, *7*, 13789. [[CrossRef](#)] [[PubMed](#)]
15. Yang, H.; Moullan, N.; Auwerx, J.; Gijs, M.A. Super-resolution biological microscopy using virtual imaging by a microsphere nanoscope. *Small* **2014**, *10*, 1712–1718. [[CrossRef](#)] [[PubMed](#)]
16. Huszka, G.; Yang, H.; Gijs, M.A. Microsphere-based super-resolution scanning optical microscope. *Opt. Express* **2017**, *25*, 86–90. [[CrossRef](#)]



17. Li, L.; Guo, W.; Yan, Y.; Lee, S.; Wang, T. Label-free super-resolution imaging of adenoviruses by submerged microsphere optical nanoscopy. *Light. Sci. Appl.* **2013**, *2*, e104. [[CrossRef](#)]
18. Lee, S.; Li, L.; Ben-Aryeh, Y.; Wang, Z.; Guo, W. Overcoming the diffraction limit induced by microsphere optical nanoscopy. *J. Opt.* **2013**, *15*, 125710. [[CrossRef](#)]
19. Yan, B.; Yue, L.; Monks, J.N.; Yang, X.; Xiong, D.; Jiang, C.; Wang, Z. Superlensing plano-convex-microsphere (PCM) lens for direct laser nano-marking and beyond. *Opt. Lett.* **2020**, *45*, 1168–1171. [[CrossRef](#)]
20. Yan, B.; Song, Y.; Yang, X.; Xiong, D.; Wang, Z. Unibody microscope objective tipped with a microsphere: Design, fabrication, and application in subwavelength imaging. *Appl. Opt.* **2020**, *59*, 2641–2648. [[CrossRef](#)]
21. Luo, H.; Yu, H.; Wen, Y.; Zhang, T.; Li, P.; Wang, F.; Liu, L. Enhanced high-quality super-resolution imaging in air using microsphere lens groups. *Opt. Lett.* **2020**, *45*, 2981–2984. [[CrossRef](#)]
22. Su, H.; Price, C.-A.H.; Jing, L.; Tian, Q.; Liu, J.; Qian, K. Janus particles: Design, preparation, and biomedical applications. *Mater. Today Bio* **2019**, *4*, 100033. [[CrossRef](#)]
23. Marschelke, C.; Fery, A.; Synytska, A. Janus particles: From concepts to environmentally friendly materials and sustainable applications. *Colloid Polym. Sci.* **2020**, *298*, 841–865. [[CrossRef](#)]
24. Aizawa, S.; Seto, K.; Tokunaga, E. External field response and applications of metal coated hemispherical Janus particles. *Appl. Sci.* **2018**, *8*, 653. [[CrossRef](#)]
25. Yue, L.; Minin, O.V.; Wang, Z.; Monks, J.N.; Shalin, A.S.; Minin, I.V. Photonic hook: A new curved light beam. *Opt. Lett.* **2018**, *43*, 771–774. [[CrossRef](#)]
26. Minin, I.V.; Minin, O.V.; Katyba, G.M.; Chernomyrdin, N.V.; Kurlov, V.N.; Zaytsev, K.I.; Yue, L.; Wang, Z.; Christodoulides, D.N. Experimental observation of a photonic hook. *Appl. Phys. Lett.* **2019**, *114*, 031105. [[CrossRef](#)]
27. Gu, G.; Shao, L.; Song, J.; Qu, J.; Zheng, K.; Shen, X.; Peng, Z.; Hu, J.; Chen, X.; Chen, M.; et al. Photonic hooks from Janus microcylinders. *Opt. Express* **2019**, *27*, 37771–37780. [[CrossRef](#)]
28. Pawar, A.B.; Kretzschmar, I. Patchy particles by glancing angle deposition. *Langmuir* **2008**, *24*, 355–358. [[CrossRef](#)]
29. Yang, S.; Cao, Y.; Shi, Q.; Wang, X.; Chen, T.; Wang, J.; Ye, Y.-H. Label-free super-resolution imaging of transparent dielectric objects assembled on a silver film by a microsphere-assisted microscope. *J. Phys. Chem. C* **2019**, *123*, 28353–28358. [[CrossRef](#)]
30. Cao, Y.; Yang, S.; Wang, J.; Shi, Q.; Ye, Y.-H. Surface plasmon enhancement for microsphere-assisted super-resolution imaging of metallodielectric nanostructures. *J. Appl. Phys.* **2020**, *127*, 233103. [[CrossRef](#)]
31. Ye, R.; Ye, Y.H.; Zhou, Z.; Xu, H. Gravity-assisted convective assembly of centimeter-sized uniform two-dimensional colloidal crystals. *Langmuir* **2013**, *29*, 1796–1801. [[CrossRef](#)] [[PubMed](#)]
32. Fang, C.; Yang, S.; Wang, X.; He, P.; Ye, R.; Ye, Y.H. Fabrication of two-dimensional silica colloidal crystals via a gravity-assisted confined self-assembly method. *Colloid Interface Sci. Commun.* **2020**, *37*, 100286. [[CrossRef](#)]
33. Sanchez, C.; Cristóbal, G.; Bueno, G.; Blanco, S.; Borrego-Ramos, M.; Olenici, A.; Pedraza, A.; Ruiz-Santaquiteria, J. Oblique illumination in microscopy: A quantitative evaluation. *Micron* **2018**, *105*, 47–54. [[CrossRef](#)] [[PubMed](#)]
34. Fan, Y.; Li, J.; Lu, L.; Sun, J.; Hu, Y.; Zhang, J.; Li, Z.; Shen, Q.; Wang, B.; Zhang, R.; et al. Smart computational light microscopes (SCLMs) of smart computational imaging laboratory (SCILab). *PhotonIX* **2021**, *2*, 19. [[CrossRef](#)]